


## Complete three-dimensional structure of Bi-adsorbed Si(110) surface: Discovery of heavily reconstructed Si(110) substrate

Hiroaki Aoyama<sup>1</sup> and Tadashi Abukawa<sup>1,2</sup>

<sup>1</sup>*Institute of Multidisciplinary Research for Advanced Materials, Tohoku University, 2-1-1 Katahira, Aoba-ku, Sendai 980-8577, Japan*

<sup>2</sup>*International Center of Synchrotron Radiation Innovation Smart, Tohoku University, 2-1-1 Katahira, Aoba-ku, Sendai 980-8577, Japan*

 (Received 5 August 2021; revised 12 October 2021; accepted 12 November 2021; published 8 December 2021)

Silicon is one of the most well-studied crystals in terms of surface structure. In particular, the three low Miller index surfaces—(100), (110), and (111)—which are located at the three apexes of the triangle of the irreducible orientation of the cubic crystal, are the most fundamental and have been extensively studied. However, the surface structure on Si(110) substrates is not as well understood as on other substrates. Here, we have investigated a surface structure induced by submonolayer Bi deposition on Si(110). The complete atomic arrangement from the surface to the fifth layer was directly determined by solving the Patterson function, which was obtained using a very large number of electron diffraction patterns. In contrast to the case of the Si(111) substrate, the Si(110) substrate showed significant reconstructions under a Bi overlayer. The obtained structure shows how dangling bonds can be reduced at the Si(110) substrate. The present result proves the high capability of the surface structure determination of the present method.

DOI: [10.1103/PhysRevResearch.3.043164](https://doi.org/10.1103/PhysRevResearch.3.043164)

### I. INTRODUCTION

The surfaces of covalent crystals such as Si and Ge are typically reconstructed to reduce unstable broken bonds, i.e., dangling bonds (DBs), created by crystal truncation. The Si(111) surface, one of the low index surfaces, is known to exhibit a surface reconstruction called the  $7 \times 7$  superstructure [1–5]. The atomic arrangement of the  $7 \times 7$  structure, including the reconstruction from the surface to the third layer, was determined by Takayanagi *et al.* in 1985 after various studies by many researchers [3,4]. Another low-index surface, Si(100), shows a centered  $4 \times 2$  superstructure in the ground state, and a buckled Si dimer model is accepted for this surface [6–10].

Despite many studies over several decades, the atomic structure of Si(110), one of the three important low-index surfaces of the cubic crystal, has not yet been determined [11–21]. A clean Si(110) surface is known to exhibit the so-called  $16 \times 2$  superstructure [11–15]. Although several structural models have been proposed to explain scanning tunneling microscopy (STM) images [16–21], no consensus has been reached for the structural models to explain a semiconducting surface electronic state [22,23]. One of the reasons is that the size of the  $16 \times 2$  unit cell is so large that hundreds of atomic positions have to be determined. Since the structure of the clean surface has not been determined yet, the surface

structures on a Si(110) substrate, such as metal adsorbed surfaces, have hardly been analyzed so far.

Here, we have investigated a surface structure induced on the Si(110) substrate by a small amount of bismuth atoms, i.e., a Si(110)-(3  $\times$  2)-Bi surface [24–26]. This would be a first step toward understanding the structure of Si(110) substrates. Bi is a heavy group-V semimetal with strong spin-orbit coupling, and it has been shown to exhibit Rashba-type spin-splitting of electronic states on the Bi adsorbed semiconductor surfaces [27,28]. Bi arrangements that qualitatively satisfy the  $3 \times 2$  periodicity have been proposed [25], and semiconducting surface states were observed recently by angle-resolved photoemission spectroscopy (ARPES) [26]. To understand Bi-induced electronic states of the surface, it is fundamental to determine the quantitative surface structure.

The adsorption of such metal atoms often terminates the DBs on the surface, which eliminates the reconstruction of the substrate. For example, 1/3 ML (1 ML corresponds to the atom density on the substrate surface) of a trivalent metal such as Al, Ga, or In terminates all DBs of Si(111) and forms a  $\sqrt{3} \times \sqrt{3}$  superstructure, by which the  $7 \times 7$  reconstruction is completely removed under the metal overlayer [29–31]. Figure 1(a) shows an ideal Si(110) surface formed by zigzag chains of Si atoms, and there are 12 surface atoms, thus 12 DBs, within a  $3 \times 2$  unit cell. Theoretically, four Bi atoms, i.e., 1/3 ML, is sufficient to terminate the 12 DBs in the unit cell, because Bi typically acts as a trivalent atom with one lone pair of electrons. However, the spacing between the zigzag chains is slightly too large to be simply bridged by a Bi atom.

We have performed a full three-dimensional (3D) structural analysis of the Si(110) $3 \times 2$ -Bi surface using electron diffraction. The structure determined by the present study is shown in Fig. 1(b). The structure unexpectedly included significant reconstructions of the substrate, and relaxation of

Published by the American Physical Society under the terms of the [Creative Commons Attribution 4.0 International](https://creativecommons.org/licenses/by/4.0/) license. Further distribution of this work must maintain attribution to the author(s) and the published article's title, journal citation, and DOI.

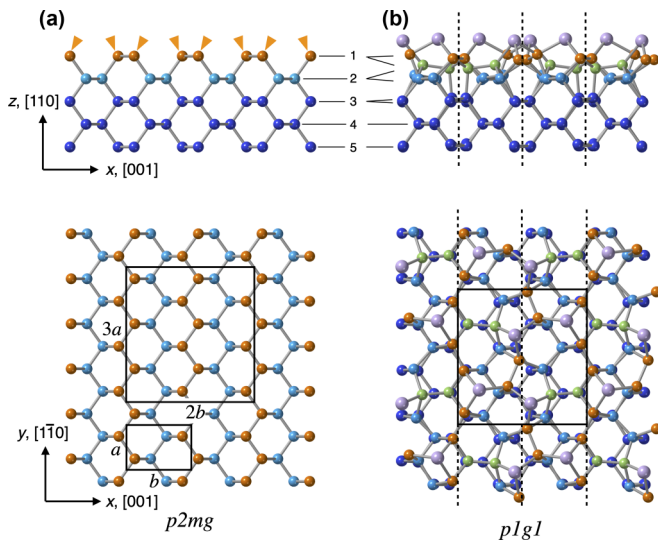


FIG. 1. (a) Side view and top view ball-and-stick model of an ideal Si(110) surface. Si atoms in the first, second, and other layers are shown as orange, light blue, and blue, respectively. Each atom in the first layer has one DB, as shown by triangles in the side view.  $1 \times 1$  and  $3 \times 2$  unit cells are shown by solid rectangles, where the  $1 \times 1$  lattice constants  $a$  and  $b$  are 3.84 and 5.43 Å, respectively. (b) The Si(110) $3 \times 2$ -Bi surface determined by the present study, where Bi atoms are shown in light purple and Si dimers connecting the first and second layers are shown in green (see the text). The dashed line shows the glide plane of the structure.

the atomic positions was observed down to the fifth layer. The DBs recombined from the ideal surface were completely terminated by Bi atoms, so that there were no DBs remaining in the structure. It is surprising that detailed atomic positions down to the fifth layer were obtained, which proves the high structure determination capability of the present method.

## II. METHODS

### A. Weissenberg method for RHEED

In the present study, we have used Weissenberg reflection high-energy electron diffraction (W-RHEED) to analyze the surface structure [32,33]. Analogous to the Weissenberg camera for x-ray diffraction [34,35], the sample was rotated about the azimuth axis  $\varphi$  in W-RHEED, as shown in Fig. 2(a). This is equivalent to the rotation of the Ewald sphere [see Figs. 2(b) and 2(c)] with respect to the fixed sample coordinate. A large volume of the reciprocal space can be surveyed by this rotation, as shown in Fig. 2(c). The sample was rotated with a small angle step, typically  $0.1^\circ$ – $0.2^\circ$ , to continuously survey reciprocal space. Usually, one of the irreducible angle ranges was scanned with a small angle step, and hundreds of diffraction patterns were measured as a function of  $\varphi$  for a single scan. The patterns were then stored in a 3D matrix with  $\varphi$  as the third dimension, as shown in Fig. 2(d). When a horizontal section is taken at  $k_z$  for the 3D matrix, as shown in Fig. 2(d), a Weissenberg photograph is obtained, where  $hk$  spots at a constant  $k_z$  are captured. If the coordinates are converted into the scattering vector  $\mathbf{s}$ , an intensity map  $I(s_x, s_y)$  is obtained from each Weissenberg photograph at the

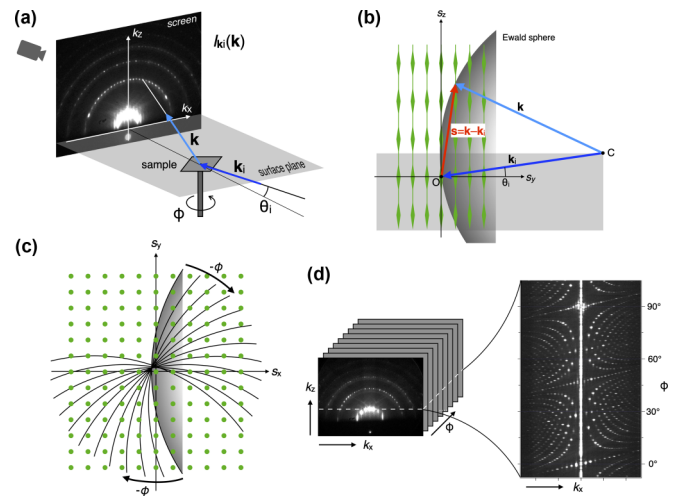


FIG. 2. Principle of W-RHEED. (a) Schematic drawing of W-RHEED measurements. The diffraction patterns were measured as a function of the sample azimuthal angle  $\varphi$ . (b) Side view of the reciprocal lattice and the Ewald sphere. The surface reciprocal lattice  $\mathbf{G}(hk, s_z)$  is schematically shown by green lines. The shaded area below C is invisible due to shadowing by the surface. (c) Top view of the reciprocal lattice. The shaded arc indicates the fraction of the Ewald sphere observed by the RHEED screen. When the sample is rotated by  $\varphi$ , the Ewald sphere is rotated by  $-\varphi$  about the crystal reciprocal space. (d) Left: A 3D matrix assembled by hundreds of RHEED patterns with the third dimension of  $\varphi$ . Right: Weissenberg photograph that is a horizontal section at a constant  $k_z$  of the 3D matrix.

constant  $s_z$ . Thus, a 3D intensity map  $I(\mathbf{s})$  is constructed from the stacks of Weissenberg photographs measured by a single scan. The surface reciprocal lattice  $\mathbf{G}(hk, s_z)$  is rendered in the experimental intensity  $I(\mathbf{s})$ . The three-dimensional Patterson function  $P(\mathbf{r})$  can be calculated by the Fourier transformation of  $I(\mathbf{s})$ .

### B. Structural analysis based on the Patterson function

The structural analysis proceeded by solving the Patterson function in the present study. Several techniques have already been developed to solve the Patterson function in x-ray crystallography [35]. To determine a structure from the Patterson function, the first step is to find a characteristic atomic cluster in  $P(\mathbf{r})$ . Since  $P(\mathbf{r})$  is the autocorrelation of the structure, the cluster is replicated at every atomic position of the structure in  $P(\mathbf{r})$ . If the cluster is appropriate, the whole surface structure can be obtained by considering the correlation between  $P(\mathbf{r})$  and the cluster.

The minimum function is a simple but effective method to evaluate the correlation between  $P(\mathbf{r})$  and the cluster [35]. The minimum function  $M(\mathbf{r})$  is defined as

$$M(\mathbf{r}) = \min\{P(\mathbf{r} - \mathbf{r}_1), P(\mathbf{r} - \mathbf{r}_2), \dots, P(\mathbf{r} - \mathbf{r}_n)\}, \quad (1)$$

where  $\mathbf{r}_i$  is the position of the  $i$ th atom that composes the cluster.  $M(\mathbf{r})$  simply picks up the minimum one from the  $P(\mathbf{r} - \mathbf{r}_i)$ 's. The only parameters required for the calculation of  $M(\mathbf{r})$  are the atomic coordinates  $\mathbf{r}_i$  of the cluster. If  $\mathbf{r}_A$  is the position of the atoms, then all  $P(\mathbf{r} - \mathbf{r}_i)$ 's have a peak

at  $\mathbf{r} = \mathbf{r}_A$ , because the cluster is replicated at  $\mathbf{r}_A$  in  $P(\mathbf{r})$ . Therefore, even the minimum of  $P(\mathbf{r} - \mathbf{r}_i)$ 's has a certain value at  $\mathbf{r}_A$ . Otherwise at least one of the  $P(\mathbf{r} - \mathbf{r}_i)$ 's should be off the peak, and  $M(\mathbf{r})$  should take a very small value. Therefore, by choosing the appropriate cluster, the positions of the atoms can be drawn directly in  $M(\mathbf{r})$ . The appropriate cluster should be unique in the whole structure and should not have an inversion symmetry.

Here, we should note the incompleteness of the reciprocal space measured by the experiment. If  $I(\mathbf{s})$  is measured for the entire  $\mathbf{s}$  space, then  $P(\mathbf{r})$  should be a positive real function. However, only the limited area can be measured; the experimental  $P(\mathbf{r})$  is the convolution of the ideal  $P(\mathbf{r})$  and the complex oscillating function that is the Fourier transformation of the experimental window function. To avoid this complex number problem,  $|P(\mathbf{r})|$  is used instead of  $P(\mathbf{r})$  in the present analysis.

Electrons are strongly scattered by atoms; therefore, the kinematical theory is usually insufficient, and the dynamical theory is required to describe electron diffraction. However, taking advantage of the ability to measure a large number of data, we could use the averaging method to reduce dynamic effects [36,37]. In the method, multiple reciprocal maps measured with different incident angles were averaged in reciprocal space in order to smear out the dynamical effect.

### III. EXPERIMENTS

#### A. Apparatus

The experiment was performed in an ultrahigh-vacuum (UHV) chamber for surface structural analysis by W-RHEED [32,33]. The base pressure of the UHV chamber was  $3 \times 10^{-9}$  Pa. The system was equipped with RHEED optics, a hemispherical electron spectrometer, a five-axis sample manipulator, a Bi evaporator ( $K$ -cell), and a quartz thickness monitor. The sample manipulator allows positioning of the sample in the  $xyz$  direction and rotation of the polar and azimuthal angles. The sample mounted on the manipulator can be resistively heated by a dc current and cooled by a cryostat in a liquid  $N_2$  flow. The RHEED optics were specially designed for W-RHEED and equipped with a retarding-field energy filter to eliminate inelastically scattered electrons from the diffraction pattern. The filter had sufficient energy resolution to remove the plasmon-loss electrons from the elastically scattered electrons [32,33,38]. For W-RHEED, only the elastically scattered electrons were measured by the filter. This guarantees that the mean path length of the observed electrons in the solid will be the electron inelastic mean free path. Thus, the surface sensitivity is improved over the nonfiltered RHEED. Furthermore, Kikuch lines, which sometimes disturb the spot measurements, were greatly reduced in the energy-filtered RHEED pattern, as reported in Ref. [38]. The diffraction pattern was displayed on a phosphor screen and captured by a CCD camera. The typical exposure time was 2000 ms for each diffraction pattern.

#### B. Preparation of the Si(110) $3 \times 2$ -Bi surface

The sample substrate was cut from a Si(110) wafer to a size of  $3 \times 20 \times 0.5$  mm. The substrate was mounted on the

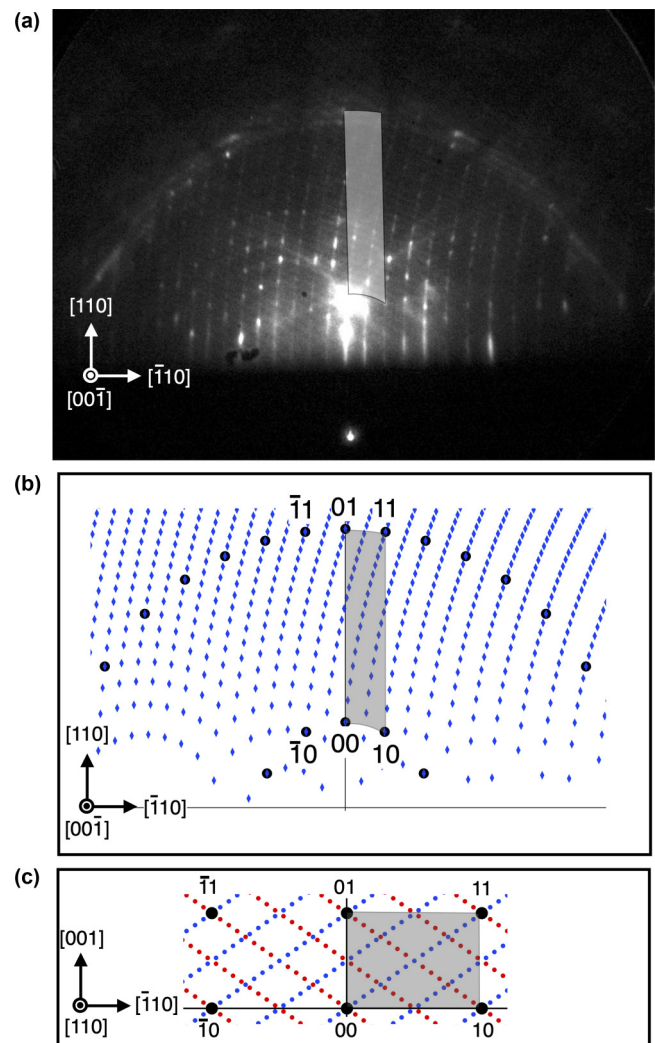


FIG. 3. (a) RHEED pattern of the single domain Si(110) $16 \times 2$  surface, where the electrons are incident along the  $[00\bar{1}]$  direction at  $\theta_i = 4^\circ$ . The shaded area indicates a reciprocal unit cell of an ideal  $1 \times 1$  lattice. (b) Simulated RHEED spot positions expected for the single domain  $16 \times 2$  lattice. (c) Top view of the lattices for two orientations of  $16 \times 2$  shown by blue and red spots. Blue spots correspond to those in (b).

manipulator and cleaned in the UHV chamber by heating to  $1250^\circ\text{C}$ . A RHEED pattern for the clean Si(110) substrate is shown in Fig. 3(a). A single domain of Si(110) $16 \times 2$  was obtained. It has been reported that a single domain  $16 \times 2$  is produced when monatomic steps run along the  $[\bar{1}\bar{1}2]$  or  $[1\bar{1}2]$  directions [39]. We have not confirmed the step orientation, but the present wafer may satisfy this condition.

While the RHEED pattern was being monitored, Bi was deposited  $\sim 1$  ML from the  $K$ -cell onto a clean Si(110)  $16 \times 2$  surface at  $450^\circ\text{C}$ . Prior to deposition, the  $16 \times 2$  pattern was still observed at  $450^\circ\text{C}$ . After a postannealing at  $450^\circ\text{C}$  for 10 min, a sharp  $3 \times 2$  pattern was obtained. RHEED patterns for the Si(110) $3 \times 2$ -Bi surface are shown in Figs. 4(a) and 4(b), which were measured after cooling to  $\sim 150$  K. The amount of Bi on the  $3 \times 2$  surface was estimated to be  $0.4 \pm 0.1$  ML by Auger electron spectroscopy and a quartz thickness monitor.

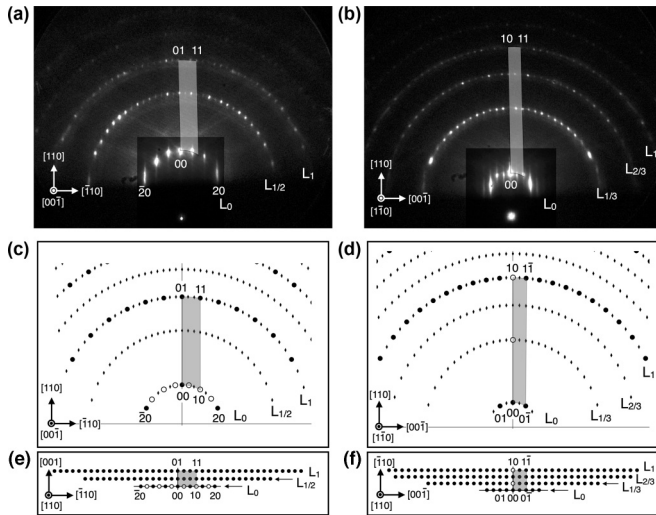


FIG. 4. (a), (b) RHEED patterns for the  $\text{Si}(110)3 \times 2\text{-Bi}$  surface observed with  $[00\bar{1}]$  incidence at  $\theta_i = 4^\circ$  and with  $[1\bar{1}0]$  incidence at  $\theta_i = 2.5^\circ$ , respectively. The shaded area indicates a  $1 \times 1$  unit cell. To avoid saturation of the strong spots, the intensity scale was suppressed to  $1/3$  around the  $L_0$  ring. (c), (d) Simulated spot positions for the patterns (a) and (b), respectively. Missing spots are indicated by open circles. (e), (f) Top views of the reciprocal lattices corresponding to (c) and (d), respectively.

### C. W-RHEED acquisition

W-RHEED was applied to the prepared  $\text{Si}(110)3 \times 2\text{-Bi}$  surface after cooling to  $\sim 150$  K. The setup for the measurements is shown schematically in Fig. 2(a). To scan the irreducible angle range, the sample azimuth angle  $\varphi$  was rotated through  $\sim 110^\circ$  that covered from  $[00\bar{1}]$  to  $[1\bar{1}0]$  at a fixed grazing angle. The sample was continuously rotated at a constant speed during the scan, and the patterns were measured every  $0.2^\circ$  in on-the-fly mode, so that 550 patterns were measured in a single scan in 20 min. In the present study, six scans were measured at different grazing incidences of  $\theta_i = 2.0^\circ, 2.5^\circ, 3.0^\circ, 3.5^\circ, 4.0^\circ$ , and  $4.5^\circ$  from the surface. All measurements were made within 6 h of sample preparation.

We obtained six reciprocal maps,  $I(\mathbf{s})$ , at different incidence angles  $\theta_i$  for the  $\text{Si}(110)3 \times 2\text{-Bi}$  surface. Projections of three-dimensional  $I(\mathbf{s})$  at  $\theta_i = 2.0^\circ, 3.5^\circ$ , and  $4.5^\circ$  are shown in Fig. 5. The horizontal projection shows that more than half of the azimuthal range was covered by the  $110^\circ$  scan. Taking into account the glide plane symmetry along the  $[1\bar{1}0]$  axis, i.e.,  $I(s_x, s_y, s_z) = I(-s_x, s_y, s_z)$ , the data were extended to the full azimuthal range. The six maps with different grazing incidences were then summed into a total intensity map  $I(\mathbf{s})$ , from which the Patterson map  $P(\mathbf{r})$  was calculated.

## IV. RESULTS

### A. RHEED patterns and Patterson function

The RHEED patterns of  $3 \times 2\text{-Bi}$  surface, shown in Fig. 4, convey two important clues regarding the structure. One is the lack of odd index spots in the zeroth Laue zone ( $L_0$ ), which indicates the presence of a glide plane symmetry along the  $y$  ( $[1\bar{1}0]$ ) direction in the structure. The other is that the spot

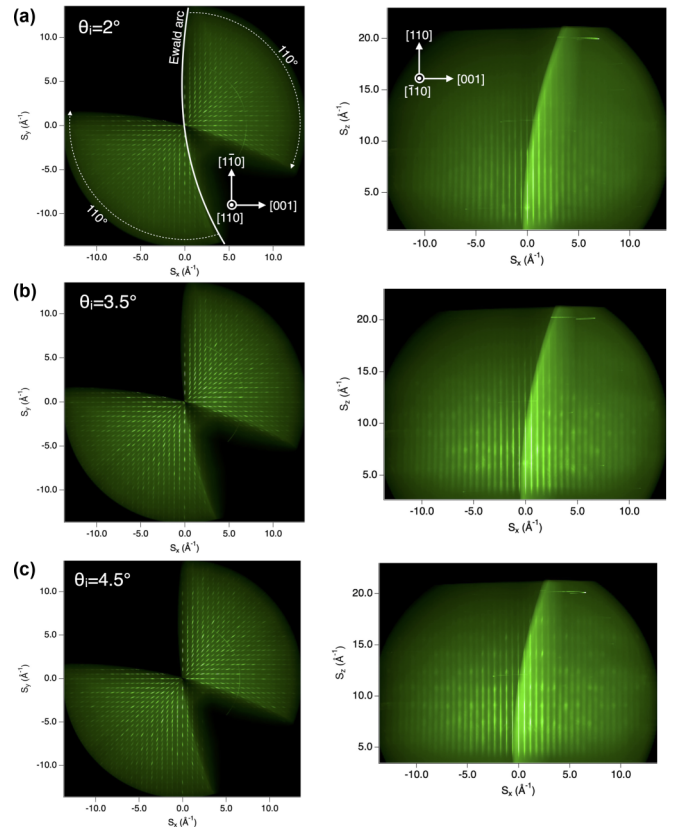


FIG. 5. Horizontal ( $xy$ ) projections (left) and vertical ( $xz$ ) projections (right) of a three-dimensional map  $I(\mathbf{s})$  obtained by each W-RHEED scan measured at (a)  $\theta_i = 2^\circ$ , (b)  $\theta_i = 3.5^\circ$ , and (d)  $\theta_i = 4.5^\circ$ , respectively. The perimeter of the Ewald sphere (Ewald arc) at the starting point is schematically shown in (a).

intensity was not symmetric about the vertical center line in Fig. 2(a), so that the surface has no mirror symmetry about the plane including the  $[001]$  and  $[110]$  axes. Therefore, it is concluded that the  $3 \times 2$  surface belongs to the surface space group  $p1g1$ .

A 3D Patterson map  $P(\mathbf{r})$  was calculated by the Fourier transformation of the total  $I(\mathbf{s})$ . A horizontal slice of  $|P(\mathbf{r})|$  at  $z = 0.0 \text{ \AA}$  is shown in Fig. 6(a), where the magnitude of  $P(\mathbf{r})$  is plotted in a  $3 \times 2$  unit cell. There are several spots in the figure that could represent the atoms. Except for the strong peak at the origin, the structure in  $P(\mathbf{r})$  at  $r < 1.5 \text{ \AA}$  should be an artifact caused by the experimental limitations, such as the limited range or inhomogeneous sensitivity of the screen because no reasonable interatomic bond smaller than  $1.5 \text{ \AA}$  is expected in the present surface. The spot size, which is inversely proportional to the size of the measured reciprocal map, was  $\sim 0.3 \text{ \AA}$  in the lateral and  $\sim 0.6 \text{ \AA}$  in the vertical directions. The small spot size is one of the key criteria for solving the Patterson function. Important slices of  $|P(\mathbf{r})|$  are shown in Fig. 7 with the simulated  $|P(\mathbf{r})|$  for the present structural model.

### B. Initial structural analysis

The dominant spots in the slice shown in Fig. 6(a) are labeled and schematically shown in Fig. 6(b). The positions

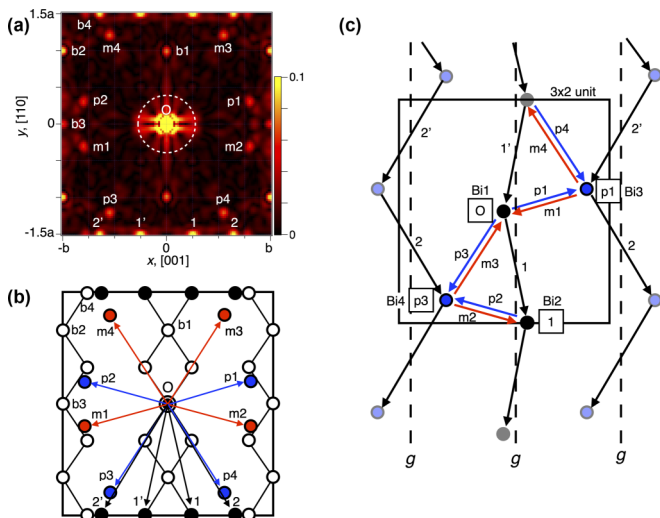


FIG. 6. (a) Horizontal section of  $|P(\mathbf{r})|$  at  $z = 0.0 \text{ \AA}$ . (b) Illustration of experimental spots observed in (a). (c) Cluster of four atoms at O, 1,  $p1$ , and  $p3$  that is solved from (a) is arranged with  $3 \times 2$  periodicity. Interatomic vectors between the four atoms are shown by blue, red, and black arrows. Broken lines indicate the glide planes in the arrangement.

expected for the ideal bulk structure are also shown by open circles. When the spot positions were investigated in three dimensions, some of the spots were  $0.2 \text{ \AA}$  off from the  $z = 0.0 \text{ \AA}$  plane. The spots labeled  $p1$ – $p4$  (blue dots in the figure) are located at  $z = 0.2 \text{ \AA}$ , and their inversion counterparts  $m1$ – $m4$  (red dots) are located at  $z = -0.2 \text{ \AA}$  [see the vertical section of  $|P(\mathbf{r})|$  in Fig. 7(b)]. On the other hand, the intense spots labeled 1,  $1'$ , 2, and  $2'$  [black dots in Fig. 6(b)] are located at  $z = 0.0 \text{ \AA}$ . The other noticeable spots ( $b1$ – $b4$ ) and their symmetric equivalents are interpreted as being associated with the bulk structure.

These surface spots in  $|P(\mathbf{r})|$  should be solved as an arrangement of atoms that satisfy  $p1g1$  symmetry. When glide planes are considered, each spot should have a counterpart that is located at a half unit ( $3a/2$ ) shift in the  $y$  direction. The positions of  $p3$  and  $p4$  were shifted by the half unit from those of  $p1$  and  $p2$ , so that they could be the counterparts of the glide symmetry. Spots 1,  $1'$ , 2, and  $2'$  could be the counterparts of the spot at the origin. When spot 1 is selected as the counterpart of the origin O, the glide plane must run vertically through its midpoint, as shown in Fig. 6(c). Then,  $p1$  and  $p3$  are automatically selected as the atomic pair that satisfies the same glide plane. Thus, four atoms at O, 1,  $p1$ , and  $p3$  shown in Fig. 6(c) can be selected as a cluster that satisfies  $p1g1$ . Using these four atoms, the spots in Fig. 6(a) are perfectly interpreted by their interatomic vectors, as shown by the arrows in Fig. 6(c). There are four possible choices for the glide counterpart of O, i.e., 1,  $1'$ , 2, or  $2'$ . However, any choice results in the equivalent arrangement of the four atoms. From here, we proceed to analyze the structure with the four atoms as Bi atoms (Bi1–Bi4), as indicated in Fig. 6(c), although it will be confirmed later by the bond lengths in the structure. The atomic positions of Bi1–Bi4 were determined from  $P(\mathbf{r})$  to be  $\mathbf{r}_1 = (0, 0, 0)$ ,  $\mathbf{r}_2 = (4.35, 1.15, 0.20)$ ,  $\mathbf{r}_3 =$

$(1.40, -5.75, 0.0)$ , and  $\mathbf{r}_4 = (-2.95, -4.60, 0.20)$  (in  $\text{\AA}$ ), respectively.

### C. Full structural analysis

In addition to the Bi overlayer, the 3D  $P(\mathbf{r})$  should include structural information down to  $\sim 10 \text{ \AA}$  from the surface by estimation from the surface sensitivity of RHEED. The coordinates of the four Bi atoms were obtained by the initial structural analysis; therefore, this Bi cluster can be used to solve the entire structure. The minimum function method was used to solve the structure. If the cluster is unique in the structure, then the entire structure will be directly unveiled in the minimum function  $M(\mathbf{r})$ .

$M(\mathbf{r})$  was calculated using the determined coordinates of the four Bi atoms. Horizontal cross sections of  $M(\mathbf{r})$  at  $z = -1.5, -2.2, -3.2, -5.1, -7.0$ , and  $-8.9 \text{ \AA}$  are shown in Fig. 8. There are several distinct spots that should represent the atoms of the structure. In the cross section at  $z = -5.1, -7.0$ , and  $-8.9 \text{ \AA}$ , which correspond to the third, fourth, and fifth layer of the substrate, respectively, spots are arranged in zigzag chains. The zigzag chain indicated that the structure below the third layer retained the bulk zigzag structure, although significant relaxation was concluded from the detailed analysis. At  $z = -3.2 \text{ \AA}$  (approximately the second layer), the spots are arranged in turned W-shapes, which resulted from the absence of one atom from the zigzag chain. This atom missing at the second layer is found in the upper plane at  $z = -2.2 \text{ \AA}$ , which is approximately the middle plane between the first and second layers. In this plane, the spots form dimers directed to approximately the  $[001]$  direction. One of the dimer atoms would come from the second layer and the other from the first layer. Above these dimers, four dimer pairs appear in the plane at  $z = -1.5 \text{ \AA}$ , which corresponds to the first layer just below the Bi overlayer.

Picking up the position of the strong spots appearing in Fig. 8 in three dimensions and arranging the atoms at these positions, the surface structure is constructed as shown in Fig. 1(b). The center of the peak position can be determined with  $0.05 \text{ \AA}$  resolution. In the present study, the three-dimensional coordinates of 62 atoms (4 Bi and 58 Si) down to the fifth layer were determined from  $M(\mathbf{r})$ . The determined coordinates for the 62 atoms are listed in Table I. (See the Supplemental Material for a 3D graphic model of the determined structure [40].)

## V. DISCUSSIONS

### A. Validity of the structure

We now discuss the validity of the obtained structure. First, it should be emphasized that there are no DBs remaining in the structure. Thus, the present model fulfills the general condition of the stable structure and is consistent with the semiconducting surface states determined by ARPES analyses [26].

The bond length and angle are also important criteria for a reasonable structure. We evaluated all bond lengths in the present structural model. The bond lengths between Bi and Si in the structure were distributed between  $2.65$  and  $2.85 \text{ \AA}$ , which are in close agreement with the sum of the covalent

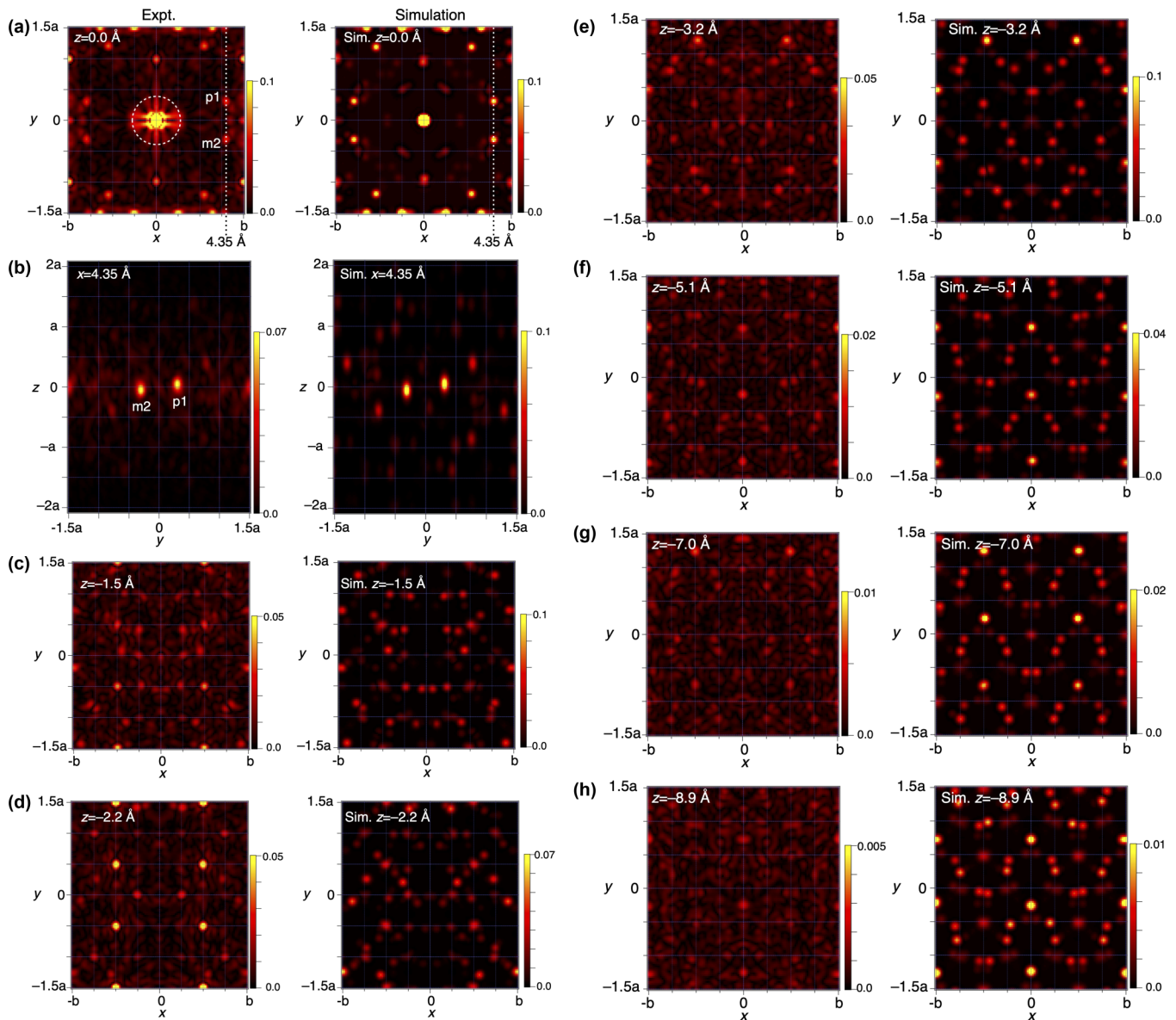


FIG. 7. Cross-sections of the experimental  $|P(\mathbf{r})|$  (left) and the simulated  $|P(\mathbf{r})|$  calculated by the present model (right). The intensity was scaled by the maximum intensity at the origin. (a) Horizontal cross-sections at  $z = 0.0 \text{ \AA}$ . (b) Vertical cross-sections on the spots  $p1$  and  $m2$  at  $x = 4.35 \text{ \AA}$ . (c)–(h) Horizontal cross-sections for  $z = -1.5, -2.2, -3.2, -5.1, -7.0,$  and  $-8.9 \text{ \AA}$ , respectively.

radii for Bi ( $1.5 \text{ \AA}$ ) and Si ( $1.18 \text{ \AA}$ ), and thus they confirm the initial assumption that the four atoms are Bi. Most of the Si-Si bonds had reasonable bond lengths between  $2.25$  and  $2.5 \text{ \AA}$ , which were close to that for the bulk ( $2.35 \text{ \AA}$ ), although two bonds had an exceptionally large bond length ( $2.7 \text{ \AA}$ ) in the unit cell [see Fig. 9(b)]. The bond directions for each Si atom were not far from the  $sp^3$  orientation in the structure. Thus, the present structure is reasonable in terms of the atomic bonding.

### B. Substrate reconstruction

Although the  $3 \times 2$ -Bi surface was experimentally reconstructed from the  $16 \times 2$  surface, the transform pathway from the ideal structure to the  $3 \times 2$ -Bi structure is fundamental to understand the reconstruction. Let us consider how the  $3 \times 2$ -Bi was reconstructed from the ideal  $1 \times 1$  structure. To

make transitions easier to understand, we considered them in a stepwise fashion. Figure 9 illustrates the proposed steps of the present reconstruction. It should be noted that these are virtually introduced steps and do not indicate a time sequence.

The Si dimer that connects the first and second layer [green atoms in Fig. 1(b)] is a characteristic component in the present structure. At the first step, this dimer would be formed from the ideal structure, as shown in Fig. 9(a); one of the bonds between the second and third layer (indicated by a red cross) is broken, and the released Si atom (black open circle in the second layer) moves upward. The neighbor of the released Si atom (black open circle in the first layer) will then move down from the first layer and make a bond with the broken bond of the third layer. As a result, one DB shifts from the first layer (dashed triangle) to the neighboring atoms in the dimer (red triangles).

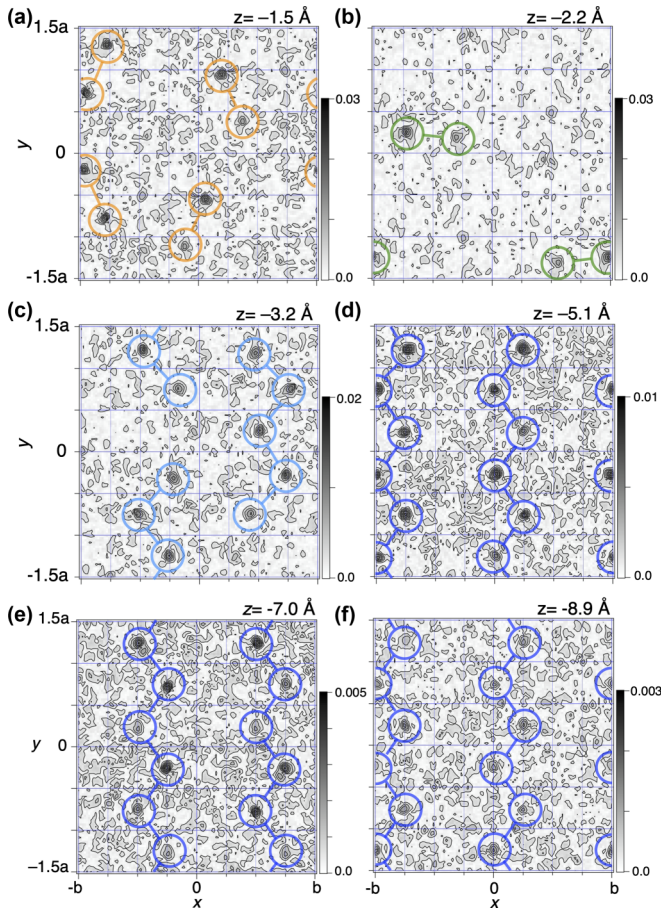


FIG. 8. Horizontal sections of  $M(\mathbf{r})$  in grayscale contour maps; (a)–(f) are sections at  $z = -1.5, -2.2, -3.2, -5.1, -7.0,$  and  $-8.9 \text{ \AA}$ , respectively. Distinct spots are surrounded by colored circles, whose colors correspond to the colors of the atoms shown in Fig. 1(b).

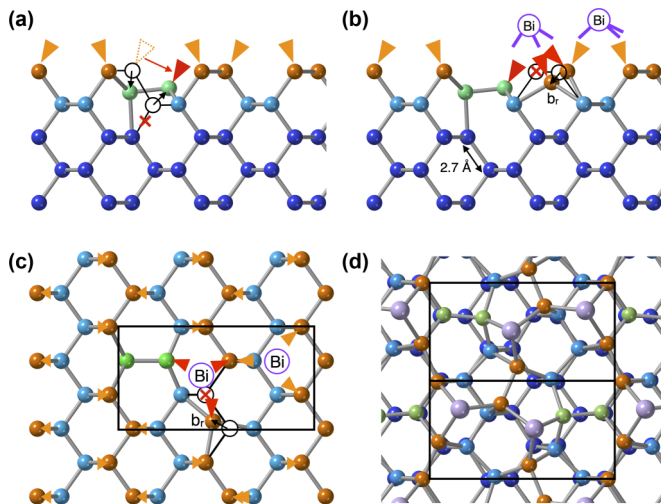


FIG. 9. Proposed pathway of the present substrate reconstruction. (a) Side view of the first step. Triangles represent DBs at the surface. (b) Side view and (c) top view of the second step. The rectangle in (c) indicates a  $3 \times 2$  half unit cell. (d) Top view of the structure determined in the present study. Note that the bond just below the dimer shown in (b) had a large bond length of  $2.7 \text{ \AA}$  in the determined structure.

TABLE I. Atomic coordinates for  $\text{Si}(110)3 \times 2\text{-Bi}$  surface. Coordinates of Bi and Si atoms down to the fifth layer of the substrate are shown ( $\text{\AA}$ ).

	Bi layer	
Bi1	(0.00, 0.00, 0.00)	
Bi2	(4.35, 1.15, 0.20)	
Bi3	(-2.95, -4.60, 0.20)	
Bi4	(1.40, -5.75, 0.00)	
	First-layer dimers	
Si1	(2.00, 1.45, -1.15)	
Si2	(-0.60, -4.30, -1.15)	
Si3	(-4.20, 5.00, -1.50)	
Si4	(-5.20, 2.80, -1.50)	
Si5	(-5.25, -0.75, -1.50)	
Si6	(-4.30, -3.00, -1.50)	
Si7	(1.05, 3.65, -1.60)	
Si8	(0.35, -2.10, -1.60)	
	Interlayer dimers	
Si9	(-1.65, 0.75, -2.05)	
Si10	(3.05, -5.00, -2.05)	
Si11	(-3.95, 0.95, -2.35)	
Si12	(5.35, -4.80, -2.35)	
	Second layer ("W" shapes)	
Si13	(-2.60, 4.70, -3.15)	
Si14	(-0.95, 2.95, -2.90)	
Si15	(-1.20, -1.20, -3.20)	
Si16	(-2.80, -2.90, -3.30)	
Si17	(-1.40, -4.80, -3.25)	
Si18	(2.55, 4.55, -3.20)	
Si19	(4.20, 2.90, -3.30)	
Si20	(2.80, 1.00, -3.25)	
Si21	(3.95, -1.05, -3.15)	
Si22	(2.35, -2.80, -2.90)	
	Third layer	
Si23	(-3.95, 4.70, -5.10)	
Si24	(-5.40, 2.85, -5.20)	
Si25	(-4.15, 0.90, -4.85)	
Si26	(5.35, -1.05, -5.10)	
Si27	(-4.10, -2.90, -5.20)	
Si28	(-5.35, -4.85, -4.85)	
Si29	(1.30, 4.75, -5.20)	
Si30	(0.00, 2.85, -5.10)	
Si31	(1.35, 0.95, -5.15)	
Si32	(0.10, -1.00, -5.20)	
Si33	(1.40, -2.90, -5.10)	
Si34	(0.05, -4.80, -5.15)	
	Fourth layer	
Si35	(-2.65, 4.80, -7.00)	
Si36	(-1.35, 2.75, -7.00)	
Si37	(-2.70, 0.85, -7.10)	
Si38	(-1.40, -1.00, -7.05)	
Si39	(-2.65, -2.90, -7.15)	
Si40	(-1.30, -4.90, -7.10)	
Si41	(2.75, 4.80, -7.05)	
Si42	(4.05, 2.85, -7.15)	
Si43	(2.70, 0.85, -7.10)	
Si44	(4.05, -1.00, -7.00)	
Si45	(2.70, -3.00, -7.00)	
Si46	(4.05, -4.90, -7.10)	

TABLE I. (Continued.)

	Fifth layer
Si47	(−4.10, 4.85, −8.75)
Si48	(−5.30, 2.80, −8.95)
Si49	(−4.05, 0.90, −8.95)
Si50	(5.40, −0.90, −8.80)
Si51	(−4.20, −2.95, −8.95)
Si52	(−5.40, −4.85, −8.95)
Si53	(1.40, 4.80, −8.95)
Si54	(0.00, 2.80, −9.05)
Si55	(1.35, 0.95, −8.95)
Si56	(0.00, −0.95, −8.95)
Si57	(1.35, −2.95, −9.05)
Si58	(0.00, −4.80, −8.95)

The second step shown in Figs. 6(b) and 6(c) might start with the removal of an atom from the first-layer atoms near the dimer (red crossed atom). This removal breaks the mirror symmetry of the substrate. The atom labeled  $b_r$  then moves in the direction toward the dimer and bridges the second-layer atoms, as shown in Fig. 6(c). In this process, the net number of DBs is unchanged from the ideal surface; however, their positions are rearranged. The rearranged DBs provide two threefold sites and are suitable to accommodate two Bi atoms. The  $3 \times 2$ -Bi structure is completed when this half unit cell is repeated to satisfy the  $p1g1$  symmetry, as shown in Fig. 9(d).

One of the bonds under the interlayer dimer atoms was experimentally concluded to have an exceptionally large bond length (2.7 Å), as shown in Fig. 9(b). It is plausible that the dimer atom that moves from the first layer pulled the atom underneath; however, theoretical evaluation is required for further discussion.

Compared to the ideal Si(110) substrate, the present substrate appears flexible with respect to relaxation of the atomic positions. The flexibility is achieved by breaking the zigzag chains of the ideal substrate without an increase in the number of DBs. The flexibility may allow the accommodation of Si atoms instead of Bi atoms. If Bi atoms are replaced by Si with tetrahedral bonds, then the number of DBs can be reduced to 1/3 of the ideal surface.

Here, we discuss the single-domain structure of the present sample. An ideal Si(110) substrate has mirror symmetry about the [001] axis; therefore, the present structure and its mirrored equivalent should take a double-domain structure on the ideal substrate. However, a single-domain  $3 \times 2$ -Bi surface was formed on the single-domain  $16 \times 2$  surface. It was reported that a single-domain  $16 \times 2$  was formed on the (110) substrate with certain regular monatomic steps [39]. The regular steps might also cause the  $3 \times 2$ -Bi single domain.

### C. Surface structural analysis by W-RHEED

In the present study, the atomic positions down to the fifth layer were directly obtained without a time-consuming trial-and-error process to evaluate assumed models. This proves the high surface structure determination capability of the present method, which is based on an analysis using a large amount of diffraction data. The result actually proves the reliability of the Patterson function obtained by W-RHEED. This is surprising because electron diffraction is usually affected by a large dynamical scattering. When the experimental  $|P(\mathbf{r})|$  is compared with the simulation in Fig. 7, most of the spots in the simulation appear as distinct spots in the experimental one. However, there are many faint structures in the background of the experiments, which should originate from the dynamical effect. These background structures had already been suppressed in the present study by the use of the averaging multiple 3D reciprocal-maps. The suppression of the background by averaging was demonstrated in the low-energy electron diffraction study of Ref. [37]. It is a great advantage of the present method that the reliable Patterson function can be obtained immediately from the experimental results. The Patterson function directly provides us with certain structural information, even if it was not completely solved. The present method is, in principle, applicable to any crystal surfaces prepared in UHV. This method provides an approach to elucidate complex surface structures.

## VI. CONCLUSION

The complete three-dimensional structure of the Si(110) $3 \times 2$ -Bi surface was solved using a vast amount of reciprocal data acquired using W-RHEED. The minimum function method was used to directly solve the complete structure using the Patterson function, and the atomic positions of 62 atoms down to the fifth layer were determined. As a result, it was found that the substrate was extensively reconstructed, even under a Bi overlayer. The formation of an interlayer Si dimer between the first and second layers is a characteristic feature of the present substrate. In the reconstruction, the dangling bonds moved from an ideal arrangement to a more concentrated arrangement suitable for termination by Bi atoms. The present study shows that complex surface structures can be solved with a large amount of diffraction data measured by W-RHEED.

## ACKNOWLEDGMENTS

This work was supported in part by the “Dynamic Alliance for Open Innovation Bridging Human, Environment and Materials” project of the Japan Ministry of Education, Culture, Sports, Science and Technology (MEXT), and by a Kakeni Grant-in Aid (No. 26105008) from the Japan Society for the Promotion of Science (JSPS).

[1] R. E. Schlier and H. E. Farnsworth, Structure and adsorption characteristics of clean surfaces of germanium and silicon, *J. Chem. Phys.* **30**, 917 (1959).

[2] G. Binnig, H. Rohrer, Ch. Gerber, and E. Weibel,  $7 \times 7$  Reconstruction on Si(111) Resolved in Real Space, *Phys. Rev. Lett.* **50**, 120 (1983).



- [3] K. Takayanagi, Structural analysis of Si(111)- $7 \times 7$  by UHV-transmission electron diffraction and microscopy, *J. Vac. Sci. Technol. A* **3**, 1502 (1985).
- [4] K. Takayanagi, Y. Tanishiro, S. Takahashi, and M. Takahashi, Structure analysis of Si(111)- $7 \times 7$  reconstructed surface by transmission electron diffraction, *Surf. Sci.* **164**, 367 (1985), and references therein.
- [5] R. Losio, K. N. Altmann, and F. J. Himpsel, Fermi surface of Si(111) $7 \times 7$ , *Phys. Rev. B* **61**, 10845 (2000).
- [6] J. Ihm, M. L. Cohen, and D. J. Chadi, ( $2 \times 1$ ) reconstructed Si(001) surface: Self-consistent calculations of dimer models, *Phys. Rev. B* **21**, 4592 (1980).
- [7] Z. Zhu, N. Shima, and M. Tsukada, Electronic states of Si(100) reconstructed surfaces, *Phys. Rev. B* **40**, 11868 (1989).
- [8] R. Felici, I. K. Robinson, C. Ottaviani, P. Imperatori, P. Eng, and P. Perfetti, Room temperature Si(001)-( $2 \times 1$ ) reconstruction solved by X-ray diffraction, *Surf. Sci.* **375**, 55 (1997).
- [9] T. Abukawa, C. M. Wei, K. Yoshimura, and S. Kono, Direct method of surface structure determination by Patterson analysis of correlated thermal diffuse scattering for Si(001) $2 \times 1$ , *Phys. Rev. B* **62**, 16069 (2000).
- [10] Y. Enta, S. Suzuki, and S. Kono, Angle-Resolved-Photoemission Study of the Electronic Structure of the Si(001)c( $4 \times 2$ ) Surface, *Phys. Rev. Lett.* **65**, 2704 (1990).
- [11] Y. Yamamoto, Study of a Si(110) surface by using reflection high-energy electron diffraction-total reflection angle X-ray spectroscopy and high temperature scanning tunneling microscopy, *Surf. Sci.* **313**, 155 (1994).
- [12] Y. Yamamoto, Atomic arrangements of  $16 \times 2$  and  $(17,15,1) 2 \times 1$  structures on a Si(110) surface, *Phys. Rev. B* **50**, 8534 (1994).
- [13] W. E. Packard and J. D. Dow, Si(110)- $16 \times 2$  and Si(110)- $5 \times 1$  surface reconstructions: Stretched-hexagon face-centered adatom model, *Phys. Rev. B* **55**, 15643 (1997).
- [14] T. An, M. Yoshimura, I. Ono, and K. Ueda, Elemental structure in Si(110)-( $16 \times 2$ ) revealed by scanning tunneling microscopy, *Phys. Rev. B* **61**, 3006 (2000).
- [15] M. Setvín, V. Brázdová, D. R. Bowler, K. Tomatsu, K. Nakatsuji, F. Komori, and K. Miki, Electronic structure of Si(110)-( $16 \times 2$ ) studied by scanning tunneling spectroscopy and density functional theory, *Phys. Rev. B* **84**, 115317 (2011).
- [16] A. I. Shkrebtii, C. M. Bertoni, R. Del Sole, and B. A. Nesterenko, Structural models of reconstructed Si(110) surface phases, *Surf. Sci.* **239**, 227 (1990).
- [17] N. Takeuchi, Bond conserving rotation, adatoms and rest atoms in the reconstruction of Si(110) and Ge(110) surfaces: A first principles study, *Surf. Sci.* **494**, 21 (2001).
- [18] A. A. Stekolnikov, J. Furthmüller, and F. Bechstedt, Long-Range Surface Reconstruction: Si (110)-( $16 \times 2$ ), *Phys. Rev. Lett.* **93**, 136104 (2004).
- [19] A. A. Stekolnikov, J. Furthmüller, and F. Bechstedt, Structural elements on reconstructed Si and Ge (110) surfaces, *Phys. Rev. B* **70**, 045305 (2004).
- [20] T. Yamasaki, K. Kato, T. Uda, T. Yamamoto, and T. Ohno, First-principles theory of Si(110)-( $16 \times 2$ ) surface reconstruction for unveiling origin of pentagonal scanning tunneling microscopy images, *Appl. Phys. Express* **9**, 035501 (2016).
- [21] R. A. Zhachuk and A. A. Shklyaev, Universal building block for (110)-family silicon and germanium surfaces, *Appl. Surf. Sci.* **494**, 46 (2019).
- [22] N. D. Kim, Y. K. Kim, C.-Y. Park, H. W. Yeom, H. Koh, E. Rotenberg, and J. R. Ahn, High-resolution photoemission spectroscopy study of the single-domain Si(110)- $16 \times 2$  surface, *Phys. Rev. B* **75**, 125309 (2007).
- [23] K. Sakamoto, M. Setvin, K. Mawatari, P. E. J. Eriksson, K. Miki, and R. I. G. Uhrberg, Electronic structure of the Si(110)-( $16 \times 2$ ) surface: High-resolution ARPES and STM investigation, *Phys. Rev. B* **79**, 045304 (2009).
- [24] H. Sakama, A. Kawazu, T. Sueyoshi, T. Sato, and M. Iwatsuki, Adsorption of bismuth on Si(110) surfaces studied by scanning tunneling microscopy, *Jpn. J. Appl. Phys.* **32**, 2929 (1993).
- [25] A. K. R. Ang, S. N. Takeda, and H. Daimon, Bi induced superstructures on Si(110), *J. Vac. Sci. Technol. A Vacuum, Surfaces, Film.* **34**, 051401 (2016).
- [26] T. Konno, R. Katsumata, A. Kimura, L. Nakamura, R. Moronuki, S. Yamazaki, K. Ozawa, K. Mase, T. Iimori, F. Komori, H. Hirayama, and K. Nakatsuji, Electronic structure of Si(110) $3 \times 2$ -Bi surface, *Annu. Meet. Jpn. Soc. Vac. Surf. Sci.* **2020**, 2Ba08 (2020).
- [27] Y. Ohtsubo, S. Hatta, K. Yaji, H. Okuyama, K. Miyamoto, T. Okuda, A. Kimura, H. Namatame, M. Taniguchi, and T. Aruga, Spin-polarized semiconductor surface states localized in subsurface layers, *Phys. Rev. B* **82**, 201307 (2010).
- [28] A. Takayama, T. Sato, S. Souma, T. Oguchi, and T. Takahashi, One-Dimensional Edge States with Giant Spin Splitting in a Bismuth Thin Film, *Phys. Rev. Lett.* **114**, 066402 (2015).
- [29] J. E. Northrup, Si(111)  $\sqrt{3} \times \sqrt{3}$ -Al: An Adatom-Induced Reconstruction, *Phys. Rev. Lett.* **53**, 683 (1984).
- [30] M. S. Finney, C. Norris, P. B. Howes, R. G. van Silfhout, G. F. Clark, and J. M. C. Thornton, An x-ray diffraction study of the Si(111) ( $\sqrt{3} \times \sqrt{3}$ ) R $30^\circ$ -indium reconstruction, *Surf. Sci.* **291**, 99 (1993).
- [31] S. Sumitani, T. Abukawa, R. Kosugi, S. Suzuki, S. Sato, and S. Kono, Photoelectron diffraction study of the surfaces of Si(111) $\sqrt{3} \times \sqrt{3}$ -Al and -In with Mo M $\zeta$  and Cr L $\alpha$  lines, *J. Electron Spectros. Relat. Phenom.* **101–103**, 245 (1999).
- [32] T. Abukawa, T. Yamazaki, K. Yajima, and K. Yoshimura, Weissenberg Reflection High-Energy Electron Diffraction for Surface Crystallography, *Phys. Rev. Lett.* **97**, 245502 (2006).
- [33] T. Abukawa and Y. Nishigaya, Structure of the Si(111)-( $5 \times 2$ )-Au Surface, *Phys. Rev. Lett.* **110**, 036102 (2013).
- [34] K. Weissenberg, Ein neues Röntgengoniometer, *Z. Phys.* **23**, 229 (1924).
- [35] For example, M. F. C. Ladd, and R. A. Palmer, *Structure Determination by X-ray Crystallography: Analysis by X-rays and Neutrons*, 5th ed. (Springer, New York Heidelberg Dordrecht London, 2013).
- [36] M. G. Lagally, T. C. Ngoc, and M. B. Webb, Kinematic Low-Energy Electron-Diffraction Intensities from Averaged Data: A Method for Surface Crystallography, *Phys. Rev. Lett.* **26**, 1557 (1971).
- [37] T. Abukawa, T. Yamazaki, and S. Kono, Fully performed constant-momentum-transfer-averaging in low-energy electron diffraction demonstrated for a single-domain Si(111) $4 \times 1$ -In surface, *e-J. Surf. Sci. Nanotechnol.* **4**, 661 (2006).
- [38] Y. Horio, Zero-loss reflection high-energy electron diffraction patterns and rocking curves of the Si(111) $7 \times 7$  surface obtained by energy filtering, *Jpn. J. Appl. Phys.* **35**, 3559 (1996).

- [39] N. K. Lewis, N. B. Clayburn, E. Brunkow, T. J. Gay, Y. Lassailly, J. Fujii, I. Vobornik, W. R. Flavell, and E. A. Seddon, Domain formation mechanism of the Si(110) ( $16 \times 2$ ) reconstruction, *Phys. Rev. B* **95**, 205306 (2017).
- [40] See Supplemental Material at <http://link.aps.org/supplemental/10.1103/PhysRevResearch.3.043164> for a 3D graphic model (COLLADA 3D file) of the determined structure.